



## Article

### Special Issue dedicated to Peter Williams

# Stable isotope and geochemical evidence for genesis of secondary copper deposits at Girilambone, New South Wales, Australia

Erik B. Melchiorre<sup>1,2\*</sup> 

<sup>1</sup>Department of Environmental Sciences, University of California, Riverside, 900 University Avenue, Riverside, CA 92521, USA; and <sup>2</sup>California State University, San Bernardino, Department of Geological Sciences 5500 University Parkway, San Bernardino, CA. 92407, USA

#### Abstract

The Girilambone copper deposit of New South Wales, Australia, serves as an end-member model for development of a classic oxidation-zone profile in an environment virtually free of both the effects of active tectonics and significant fluctuation in the local water table. The oxidation zone of other copper deposits may be interpreted for history of recently active tectonics, palaeoclimate, and water-table stability by comparison to the Girilambone deposit. Unlike the oxidation profiles of porphyry copper deposits of western North America, which have been overprinted by many water-table fluctuations produced by active tectonics, the Girilambone deposit appears to have little modification to the original oxidation profile. Oxidation of primary sulfides at Girilambone was an exothermic process facilitated by chemolithotrophic bacteria, recorded by malachite oxygen isotope thermometry estimates of up to 52°C, and very light malachite carbon isotope values. The bacteria generated CO<sub>2</sub> which migrated upwards to react with copper rich meteoric fluids of the vadose zone to precipitate malachite. Unlike porphyry copper deposits of western North America which experienced recent tectonic activity, the secondary minerals (clays, iron oxides and copper carbonates) at Girilambone were not repeatedly fractured and offset during oxidation to re-establish permeability. This reduced permeability of the oxidation zone and slowed the release of CO<sub>2</sub> from the system, producing significantly elevated partial pressure of CO<sub>2</sub>, sufficient for azurite formation to dominate. Azurite oxygen and carbon isotope values indicate formation at lower temperatures up to 32°C, and with less bacterial activity than for malachite. The sulfide-digesting bacteria at Girilambone were relatively free of seasonal swings in population, as the deposit does not have the interbanded azurite and malachite typical of episodic bacterial populations triggered by seasonal precipitation. Thus the absence of significant Cu-carbonate banding at Girilambone serves as a palaeoclimate indicator. Deeper in the Girilambone oxidation zone, native copper and cuprite dominate, whereas chalcocite formed an enrichment blanket just above and at the modern water table. Oxygen and carbon isotope values for pseudomorphs of malachite after azurite indicate that these were generated as a retrograde reaction when CO<sub>2</sub> production from bacterial digestion of sulfides waned and temperatures in the oxidation zone were near ambient. In the post mining environment, chloride-rich groundwater seeps actively precipitate atacamite, while exposed remnants of sulfide masses form an outer rind of porous malachite. Exceptions to this oxidation zone sequence occur due to localised fluid channelisation and perched water-table lenses that generated mineralogical overprints.

**Keywords:** Girilambone, copper, malachite, azurite, oxidation zone

(Received 3 October 2021; accepted 14 January 2022; Accepted Manuscript published online: 28 January 2022; Associate Editor: Casey Bryce)

#### Introduction

##### Background

The Girilambone copper deposits of New South Wales (NSW), Australia are noted for well-crystallised specimens of azurite, malachite, native copper and cuprite. These deposits are located ~45 km north-west of Nyngan and 100 km east-north-east of

Cobar, NSW (Fig. 1). The focus of the present study is on the Girilambone (31°15'30.0797"S, 146°52'14.1934"E) and Girilambone North (31°13'19.4131"S, 146°50'54.1273"E) deposits, and excludes the Budgery, Budgerygar, Tritton and Great Hermidale deposits located to the southwest. The Girilambone deposit was mined in the Murrawombie pit, while the Girilambone North deposits were mined in the Hartmans, Larsens East, and Northeast pits (Fig. 2).

The Girilambone copper deposit was discovered initially by Thomas Hartman in 1875, and later pegged as 40 acres of mining claims in 1879 by Hartman, Charles Campbell, George Gibb, and George Hunter (McQueen, 2018). Hartman, Campbell and Gibb had previously discovered copper deposits in the Cobar district (Carne, 1908). Mining at the main Girilambone deposit

\*Author for correspondence: Erik B. Melchiorre, Email: [emelch@csusb.edu](mailto:emelch@csusb.edu)

This paper is part of a thematic set that honours the contributions of Peter Williams  
Cite this article: Melchiorre E.B. (2022) Stable isotope and geochemical evidence for genesis of secondary copper deposits at Girilambone, New South Wales, Australia. *Mineralogical Magazine* 86, 634–643. <https://doi.org/10.1180/mgm.2022.8>

© The Author(s), 2022. Published by Cambridge University Press on behalf of The Mineralogical Society of Great Britain and Ireland. This is an Open Access article, distributed under the terms of the Creative Commons Attribution licence (<http://creativecommons.org/licenses/by/4.0/>), which permits unrestricted re-use, distribution and reproduction, provided the original article is properly cited.

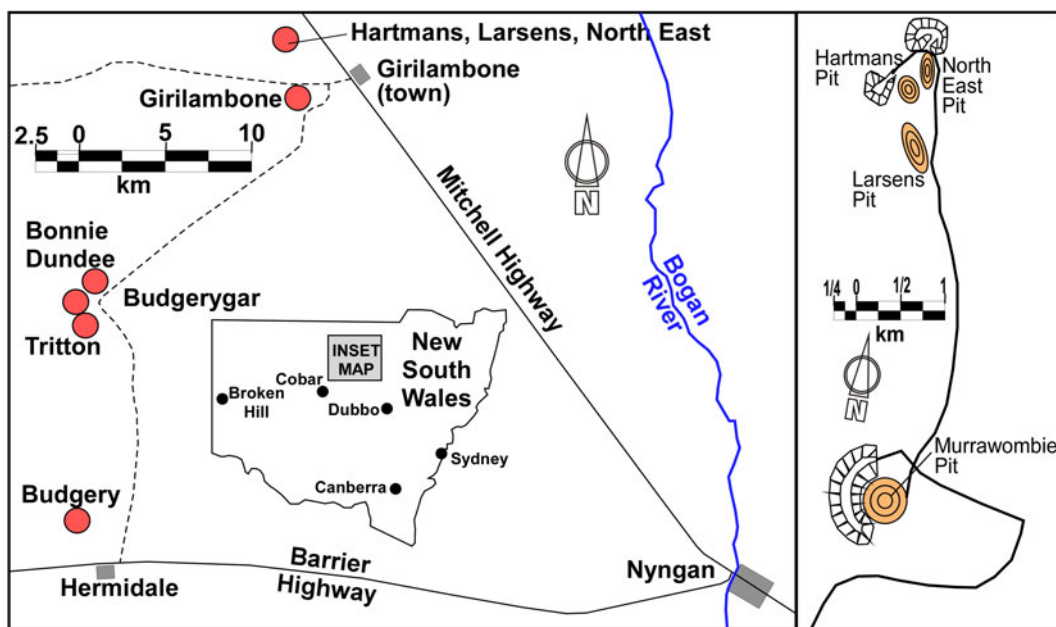


**Fig. 1.** Index map of the study area. The map on the left shows the location of the study area within New South Wales (inset) and at the regional level. Red dots show copper deposits mentioned in this study. The map on the right shows the spatial relationships of the main copper deposits at Girilambone at finer detail. Tan ovals show the location of major open pit mines and adjoining low-grade stockpiles.

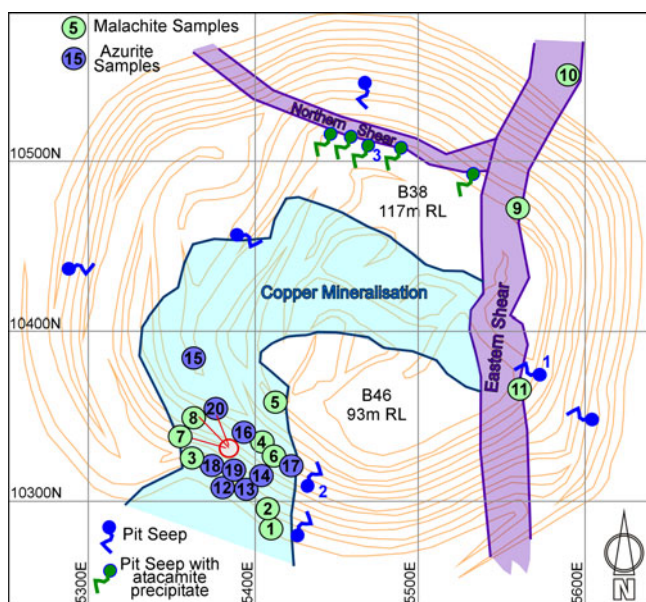


**Fig. 2.** Detailed map of the Muriwombie pit, showing locations of malachite (green dots) and azurite (blue dots) samples presented in this study. The purple zones highlight the Northern and Eastern Shear Zones, while the pale blue zone shows the mine ore zone at 1.4% Cu cut-off from 1998. Key elevations are listed and brown lines show bench levels, not topographic relief. Blue spring symbols show location of major pit-water seeps, while green spring symbols show locations of active atacamite precipitation.

commenced in 1880, and takes its name from the locality which translates to ‘place of falling stars’ in the Wielwan Aboriginal language (McQueen, 2018). Initial operations by two separate companies were limited to shallow workings (<75 m) and yielded 42 tons of copper from 3100 tons of ore between 1880 and 1884 (Carne, 1908). In 1896 the mine was re-opened by

Girilambone Copper Mining Company Limited and in the next 11 years produced ~1,142 tons of copper (Chapman *et al.*, 2005).

The deposits were largely idle until 1963–1973 when Utah Development Company explored Girilambone and delineated a 3.3 Mt resource averaging 2.12% Cu (Fogarty, 1996, 1998). Similarly, Australian Selection Party Limited identified a 1.5 Mt resource averaging 1.8% Cu between 1974 and 1983 at Girilambone North (Fogarty, 1996, 1998). In 1989 Nord Pacific Limited purchased the Girilambone deposits and identified 8 Mt of leachable copper reserves averaging 1.4% Cu, and in 1991 began mining operations as a joint venture with Straits Resources. The Murrawombie pit was started in 1992, and followed by exploitation of Girilambone North with the Northeast, Hartmans and Larsens East pits. Extraction of leachable copper between 1993 and 2002 was from a heap leach solution-extraction/electrowinning operation that yielded 115,063 tons of copper, though additional production from primary ore continued at the mill plant at the Tritton Mine (Straits Resources, 2003). The extraction of ore from underground operations at the Northeast and Larsen underground mines continued through 2016, when Murrawombie underground operations were initiated by the successor of Straits Resources, Aeris Resources. Murrawombie underground has yielded at least 500,000 tons of ~2% Cu ore, and has an estimated resource of 5.1 Mt at ~1.5% Cu for 75,000 tons of copper metal (Aeris Resources, 2021).

**Geological and mineralogical setting**

The Girilambone deposits have been described in detail for geology (Fogarty, 1996, 1998; Shields, 1996; Aeris Resources, 2021) and mineralogy (Crane *et al.*, 2001; Chapman *et al.*, 2005). Economic mineralisation is restricted to the basal unit of the Girilambone Group, the Caro schist. The Ordovician Girilambone Group is a sequence of schist, phyllite, greywacke

and quartzite. Caro schist includes sericite schist, chlorite schist, graphite schist and a 'pink quartzite' that is closely linked with the primary mineralisation of the deposit.

The simple geology of the deposit has been complicated by subsequent structural events, and metamorphism and secondary enrichment/remobilisation. Two main periods of deformation include a folding of the pink quartzite into a broad and steeply plunging syncline which flattens with depth to the southeast. Subsequent brittle deformation produced the 'Eastern Shear' which is a steeply dipping normal fault. This fault is a zone of quartzite lenses within a matrix of hematite + chlorite schist and hosts significant secondary mineralisation and most of the original underground workings of the late 1800s to early 1900s (Shields, 1996).

The mineralogy of the deposit has been described in detail by Chapman *et al.* (2005). Primary sulfide mineralisation includes layered, banded and massive pyrite and chalcopyrite within the pink quartzite, and disseminated pyrite and chalcopyrite within the lower pink quartzite and in the footwall schist. Some of the sulfide zones are reported as lenses up to 250 m by 45 m and open with depth (Fogarty, 1998). Minor lead, zinc, silver and gold are associated with the sulfide zones (Chapman *et al.*, 2005).

This primary sulfide mineralogy has been deeply weathered to produce a 'classical copper oxidation zone' (e.g. Williams, 1990). At the surface, the pink quartzite weathered to produce a siliceous gossan that was more resistant to erosion than the surrounding units. This zone has voids, surrounded by massive iron and manganese oxide minerals. These voids are host to well-crystallised secondary minerals, especially those of copper. An assemblage of copper phosphate minerals overprint this zone, with an unusual profile of decreasing libethenite and increasing pseudomalachite with depth, probably resulting from the intensity of weathering of phosphate-bearing gangue minerals (Crane *et al.*, 2001). The oxidation zone is intensely leached in the upper 30 m, and extends to the water table at ~90 m depth. A supergene enrichment blanket consisting chiefly of earthy and sooty chalcocite extends below the modern water table.

The pronounced zonation relative to the occurrence of specific secondary copper minerals is germane to the present study. This zonation was first documented by Shields (1996), who encouraged the author to study the origins of this zonation in the Murrawombie, Larsens and Northeast pits during fieldwork in 1997–1998. Malachite dominates the upper oxidation zone by Bench 5 (Reference Level 216 m), and is the most abundant secondary copper mineral in the deposit (Chapman *et al.*, 2005). Malachite and pseudomorphs of malachite after azurite occur sporadically below this, where azurite begins to dominate. Azurite increases in abundance with depth, until it becomes the major ore mineral by Bench 21 (Reference Level 168 m). Azurite was not observed below Bench 35 (Reference Level 126 m). Native copper first appears in abundance below Bench 22 (Reference Level 165 m) and persists to about Bench 40 (Reference Level 111 m).

The regional weathering history is important in understanding the potential weathering history of the Girilambone deposit. Age determination of weathering profiles in the region includes palaeomagnetic dating of hematite fixation and Ar/Ar radiometric dating of manganese oxides (table 2 in McQueen *et al.*, 2008; Smith *et al.*, 2009). These studies indicate a prolonged period of weathering from at least the Palaeocene and possibly the latest Cretaceous. This period experienced at least two major periods of deep chemical weathering under wet conditions followed by

drying of profiles, with intense oxidative deposition and fixation of hematite. Evidence for these periods of weathering are preserved at a number of the ore deposits in the region, including at the McKinnons, New Cobar, Elura (Endeavor) and Mt Boppy deposits (McQueen *et al.*, 2008).

### Context of study

In May 1997 the author was fortunate to join Peter Williams, Jim Sharpe and Bernie Day on an expedition to examine copper deposits in Central Queensland. Over the next month we visited many deposits and planned future work at Cobar and Girilambone. However, Peter Williams was unable to join me for a visit to Girilambone in June or for a visit the next year when I returned for two more weeks of field work. Girilambone remains the only Australian copper deposit of significance that I have not visited with Peter. The 1997–1998 field seasons were generously supported by mine geologist Phil Shields and Straits Resources. Phil was very interested in the zonation of different secondary copper species within the deposit, and suggested stable isotope analyses to examine the conditions of formation. While field work was underway, significant deposits of well-crystallised copper mineralisation were encountered in all three active pits at Girilambone. On return to Sydney after this field work, Peter offered to store my samples and field gear in his garage until I returned for the 1999 field season. There the samples remained for years, until Peter was instructed to clean the garage, and shipped the samples to the author in 2003. The samples remained in the original shipping boxes until finally analysed in 2018.

### Materials and methods

The sample suite for this study includes 24 carbonate mineral separates collected from high-grade surface benches (1997–1998) to obtain a representative suite of the principal copper carbonate minerals in cross-section throughout the depth of the pits as they were exposed in 1997–1998 (sample locations and elevation data Table 1; Figs 2 and 3). Raw samples had a mass of 10 to 250 grams each. To avoid analysis of impurities, samples were hand-picked from crushed and washed fractions. Only pure separates of each mineral phase were analysed.

Splits of these samples were mounted on epoxy resin to produce polished sections for microscopic observations and geochemical measurements. The surface of each polished section was examined by optical microscope (Zeiss AxioImager M2m) to obtain images for navigation under the Scanning Electron Microscope (SEM) with correlative microscopy. Mineral stoichiometry anticipated from optical observations was measured using a Zeiss (Sigma 200) field emission gun SEM equipped with two Bruker xFlash X-ray energy dispersive spectrometers (EDS) at Washington University in St. Louis, Missouri, USA. The SEM-EDS analyses used a probe current of 2.3 nA with an accelerating voltage of 20 kV at a working distance of 8.5 mm. Manual spot analysis was performed to confirm mineralogy.

Carbon and oxygen isotope analyses were performed at California State University Long Beach on hand-picked copper carbonate minerals. Analytical precision ( $1\sigma$ ) was calculated on the basis of multiple measurements of well-characterised carbonate standards between sample runs and was better than 0.05‰ for  $\delta^{13}\text{C}$  and 0.04‰ for  $\delta^{18}\text{O}$ , after corrections for scale compression. Isotopic data are reported here relative to the Vienna Standard Mean Ocean Water (V-SMOW) for oxygen and to Vienna

**Table 1.** Sample stable isotope and thermometry values from this study. Sample numbers correspond to Figs 2 and 3. Sample elevation (RL) is metres above sea level.

Sample #	Sample type	Notes	RL elevation (m)	Mine bench	$\delta^{18}\text{O}$ (V-SMOW)	$\delta^{13}\text{C}$ (V-PDB)	Thermometry estimate ( $^{\circ}\text{C}$ )
1	Malachite	Velvet malachite on black iron matrix from Mark Welch, sample GMM-1	216	5	26.90	-13.63	33
2	Malachite	Velvet malachite on black iron matrix from Phil Shields	210	7	26.43	-12.21	35
3	Malachite	Girilambone mine Bench 12, malachite balls	195	12	27.05	-11.68	32
4	Malachite	Massive malachite vein with white clay, from bench floor, Sample A-G4 from Melchiorre <i>et al.</i> (1999)	147	28	26.72	-10.78	34
5	Malachite	Malachite from nodule growing on native copper	111	40	26.57	-10.86	35
6	Malachite	Murrawombie pit berm 28, bench face (top of ladder) Girilambone mine, NSW	147	28	26.87	-10.37	33
7	Malachite	Malachite crystal on red iron-rich clay matrix from same hand sample as #8 and #20	153	26	26.32	-10.40	36
8	Malachite	Pseudomorph after azurite on red iron-rich clay matrix from same hand sample as #7 and #20	153	26	29.41	-6.57	21
9	Malachite	Malachite on massive sulfide sample	117	38	23.84	-15.16	50
10	Malachite	Malachite on massive sulfide sample from old underground workings near surface	218	NA	23.55	-14.49	52
11	Malachite	Malachite on massive sulfide sample near pit wall weep-hole	111	40	24.08	-14.92	49
12	Azurite	Thin 5 mm azurite veinlet on black iron matrix from Mark Welch, sample GMM-2	210	7	30.33	-10.14	27
13	Azurite	1 mm azurite crystals on black iron matrix from Phil Shields	204	9	30.58	-9.37	26
14	Azurite	From single 5 mm azurite crystal on white quartz	162	23	30.18	-9.78	28
15	Azurite	4 mm azurite crystals on decomposed schist	141	30	29.50	-10.22	31
16	Azurite	From two separate 6 mm azurite crystals in a white clay matrix	147	28	29.40	-9.84	32
17	Azurite	8 mm azurite crystal on white clay and black iron oxides from bench face at top of ladder, sample A-G9 from Melchiorre <i>et al.</i> (2000)	147	28	29.70	-9.51	30
18	Azurite	From single 6 mm azurite crystal on red clay and decomposed schist	183	16	29.96	-9.42	29
19	Azurite	4 mm azurite crystals on brecciated white quartz with black iron oxides	171	20	30.27	-9.28	27
20	Azurite	Azurite crystal on red iron-rich clay matrix from same hand sample as #7 and #8	153	26	30.05	-9.96	28
21	Malachite	North East pit, 2 mm acicular crystals on red and white clay	177	18	26.50	-10.42	35
22	Malachite	North East pit, veinlets in red clay	159	24	27.11	-10.94	32
23	Azurite	North East pit, two 5 mm crystals on red and white clay	177	18	29.62	-10.06	31
24	Azurite	North East pit, 3 mm crystals as druse on red clay	159	24	29.86	-11.13	29

PeeDee Belemnite (V-PDB) for carbon (Coplen, 1995). Oxygen isotope data have been converted to temperature estimates using the isotope thermometer of Melchiorre *et al.* (1999) for malachite and Melchiorre *et al.* (2000) for azurite. Similar work has been long established for thermometry of carbonate minerals (e.g. Bowen, 1966). For these calculations, groundwater that the carbonates formed from was assumed to have an oxygen isotope value of  $-4.5\text{‰}$ , on the basis of both modern groundwater values from pit seeps (Table 2) and fluid-inclusion extrapolations, consistent with values reported in Melchiorre *et al.* (2000). Thermometer reproducibility was checked by replicate analysis of laboratory standards and was better than  $\pm 0.08\text{‰}$  ( $1\sigma$ ) for oxygen isotope analyses.

Pit water samples were collected from surface seeps in the mine. Electrical conductivity (EC), pH, Eh and water temperature were measured *in situ* with portable meters. Water samples were filtered with  $0.5\mu$  filters and divided into two 250 ml glass bottles with Teflon closures. The bottle for cation analyses was acidified with 1 ml concentrated  $\text{HNO}_3$  and the bottle for anion analyses was not acidified. Sample bottles were new triple-rinsed cleanroom-grade containers. Nitric acid was added using disposable polyethylene pipettes. Cation and anion concentrations were determined by standard inductively coupled plasma optical emission spectrometry methods at the Australian Bureau of Rural Science under contract to Strats Resources. Reproducibility is better than  $\pm 5\%$  for all elements. Stable isotope analyses for waters were prepared using the  $\text{CO}_2$  equilibration method for oxygen (Epstein and Mayeda, 1953) and the zinc reduction

method (Coleman *et al.*, 1982). Results are reported in the usual  $\delta$  notation relative to the V-SMOW standard. Precision is  $0.1\text{‰}$  for oxygen and  $1\text{‰}$  for hydrogen. Analyses were performed on a Delta Plus Advantage stable isotope ratio mass spectrometer at California State University San Bernardino, USA.

In addition to the above samples, a sample of atacamite-group minerals was collected from where there was active precipitation from pit seep waters from the face of Bench 37 (114 m). This sample was collected from dry crusts and preserved in a borosilicate glass bottle with a Teflon seal closure. Mineral stoichiometry was measured using SEM-EDS at Washington University in St. Louis, Missouri, USA, as detailed for the rock samples above. Manual spot analysis was performed to confirm suspected mineralogy. Crystal system observations were inconclusive for specific identification, and detailed crystallographic work was not performed to distinguish between atacamite and clinoatacamite. Preparation for isotope analysis follows the methodology outlined in Eggenkamp *et al.* (1994). Chlorine stable-isotope analyses were performed by reacting 10 mg of the atacamite with 10 ml of 50% nitric acid for 24 hours. The resulting solution contained dissolved atacamite with no detectable non-soluble residues. This fluid was diluted with 100 ml cleanroom-grade deionised water. An aliquot of sample was reacted with  $\text{AgNO}_3$  to produce  $\text{AgCl}$ . The  $\text{AgCl}$  product was removed by filter and dried before reacting with excess  $\text{CH}_3\text{I}$  under vacuum at  $80^{\circ}\text{C}$  to produce  $\text{CH}_3\text{Cl}$ . Surplus  $\text{CH}_3\text{I}$  was removed from the  $\text{CH}_3\text{Cl}$  using a gas chromatograph column prior to analysis on a Thermo-Scientific Model252 stable isotope ratio mass

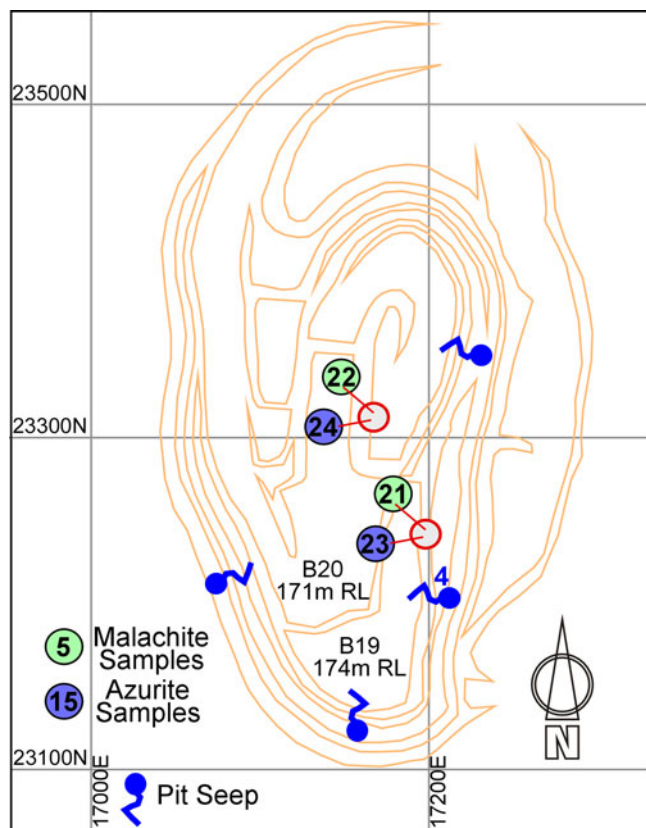


**Fig. 3.** Detailed map of the North East pit, showing locations of malachite (green dots) and azurite (blue dots) samples presented in this study. Key elevations are listed and brown lines show bench levels, not topographic relief. Blue spring symbols show location of major pit-water seeps.

spectrometer set up as a continuous-flow isotope ratio spectrometer at the University of California Riverside Facility for Isotope Ratio Mass Spectrometry (FIRMS). Measurement on sample unknowns were corrected to three standards obtained from University of Texas at Austin, and are reported in delta notation as  $\delta^{37}\text{Cl}$  relative to Standard Mean Ocean Chloride (SMOC). Reproducibility, on the basis of replicate analyses and standards is estimated at  $1\sigma$  of  $\pm 0.5\text{‰}$ .

## Results

Carbon stable-isotope values for malachite from the Girilambone main pit range from  $-15.2$  to  $-10.4\text{‰}$ , whereas azurite values range from  $-10.2$  to  $-9.3\text{‰}$  (Table 1; Figs 2 and 3). Oxygen stable-isotope values for malachite from the Girilambone main pit range from  $23.6$  to  $29.4\text{‰}$ , whereas azurite values range from  $29.4$  to  $30.6\text{‰}$  (Table 1). Oxygen isotope thermometry estimates using the isotope thermometer of Melchiorre *et al.* (1999) for malachite

and Melchiorre *et al.* (2000) for azurite yield temperatures ranging from  $21$  to  $52^\circ\text{C}$  (malachite) and  $26$  to  $32^\circ\text{C}$  (azurite). Samples from the North East pit yielded results within these same ranges.

The four pit seep samples have elevated (above drinking water standards) electrical conductivity (EC) with a near neutral pH (Table 2; Figs 2 and 3). Regional EC and pH values range from  $7200$  to  $3160 \mu\text{S}/\text{cm}$  and pH  $6.4$ – $7.1$  (Khider and McPhail, 2005) while pit seep waters range from  $30,000$  to  $19,500$  and  $7.0$  to  $7.7$ , respectively. These waters are dominated by sodium and chloride, with elevated magnesium and sulfate. Pit water sample 3, a site of active atacamite precipitation, has the most elevated chloride and copper levels. Stable isotope analyses of the waters indicate  $\delta^{18}\text{O}$  (V-SMOW) averages of  $-4.5\text{‰}$  and  $\delta\text{D}$  averages  $-35.9\text{‰}$  (Table 2). These values plot below the meteoric water line in the field of evaporative concentration. Chlorine isotope results for the atacamite sample collected from pit seep 3 (1 sample, analysed in triplicate) were  $\delta^{37}\text{Cl}$  (SMOC) of  $+0.15\text{‰}$ ,  $+0.35\text{‰}$  and  $+0.25\text{‰}$ , with an average of  $+0.25\text{‰}$ .

## Discussion

### Mineral zonation

While individual copper mineral species are known to occur as traces at all depths in the oxide zone, distinct zonation of these species is observed with depth at the Girilambone deposits (e.g. Chapman *et al.*, 2005; this study). Malachite was observed to dominate nearer the surface, but decreases in abundance as the water table was approached. The pre-mining water table is reported at being “encountered at 325 foot depth” (99 m) from the surface (McQueen, 2018). Fieldwork in 1997 and 1998 shows that azurite gradually becomes one of the main copper ore minerals by Bench 18 (177 m) and remains so until about Bench 30 (141 m). At these latter depths cuprite and native copper increase in abundance until the chalcocite enrichment blanket is encountered near the water table. This generalised mineralogical sequence with depth is illustrated in Fig. 4. Localised variations to this sequence occur where fractures and perched water table lenses create pit seeps above the regional water table. In some locations, overprinting of copper mineral species suggests a more complex localised oxidation zone history produced by fluctuations in water table levels.

### Oxygen isotope thermometry

The results of oxygen isotope analyses may be interpreted as temperatures of mineral formation. The thermometry estimates for azurite suggest temperatures of formation between  $26$  and  $32^\circ\text{C}$  (Table 1; Fig. 5), with temperatures generally increasing with depth. Malachite thermometry estimates present a more complex picture. Malachite formation temperatures show a similar trend of increasing with depth. However, the pseudomorph of malachite

**Table 2.** Water sample results for pit weeps. Sample numbers correspond to Figs 2 and 3.

Sample #	Water temperature (°C)	pH	EC (mS/cm)	Ca (mg/L)	Mg (mg/L)	Na (mg/L)	K (mg/L)	HCO <sub>3</sub> (mg/L)	SO <sub>4</sub> (mg/L)	Cl (mg/L)	Cu (mg/L)	Fe (mg/L)	$\delta^{18}\text{O}$ (V-SMOW)	$\delta\text{D}$ (V-SMOW)
1	19.5	7.1	26,600	280	950	5600	45	835	2600	8250	0.22	0.5	-4.45	-35.9
2	18.8	7.3	25,500	140	675	5500	18	910	2590	7800	0.12	0.5	-4.60	-35.2
3	20.1	7.0	30,000	320	690	7000	75	780	3500	11,200	2.50	0.8	-4.37	-36.1
4	19.3	7.7	19,500	190	750	3250	48	725	1900	5800	0.75	6.5	-4.56	-36.5

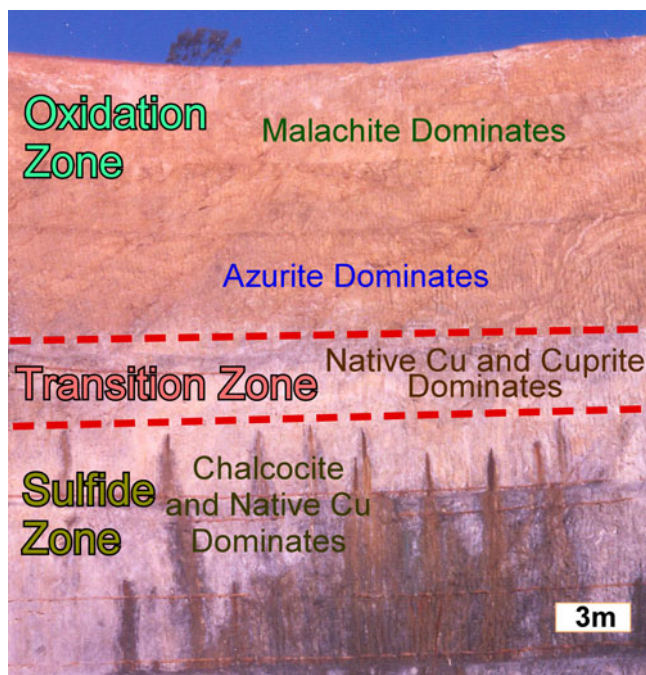


**Fig. 4.** Photograph of a characteristic pit cross section through the Girilambone main deposit exposed by the Muriwombie pit. Scale bar of 3 m is approximate due to photography angle distortion across the image.

after azurite yielded a temperature estimate below this trend (21°C) while malachite growths on massive sulfide samples had temperatures of apparent formation much higher (49–52°C). When these special case samples are removed temporarily from the dataset, the remaining ‘main trend’ malachite samples range from 32 to 36°C (Fig. 5). The results of all malachite thermometry estimates suggest at least three generations of malachite formation: (1) higher temperature (~50°C) due to exothermic decomposition of sulfides. One of these samples came from shallow 1800s mine workings in the upper oxidation zone, while the other two came from deep in the active pit operations and have malachite that clearly formed post-mining. (2) Moderate temperatures (~33°C) for most ‘main trend’ malachite. (3) Lower temperature (~21°C) as late-stage retrograde mineralisation. Significantly, the trends of increasing temperatures of malachite and azurite formation with depth converge at the depth at which the regional water table was encountered (~100 m below the pre-mining surface). This divergence in apparent formation temperatures for these two minerals at the same depths suggests that malachite and azurite may not have formed contemporaneously, but rather at different times during oxidation.

#### Carbon isotope values and carbon sourcing

Carbon isotope fractionation for malachite and azurite is known to be insensitive to temperature variation, making it an ideal tracer for identification of carbon sources (Melchiorre *et al.*, 1999, 2000). Carbon isotope tracing has identified probable carbon sources such as metal-metabolising chemolithophile bacteria at Morenci, Arizona, USA (Melchiorre and Enders, 2003) and Great Australia, Queensland, Australia (Melchiorre and Williams, 2001) while other deposits suggest deep formation fluids (Melchiorre *et al.*, 2017) and dissolution of local carbonate rocks (some samples reported in Melchiorre and Enders, 2003).

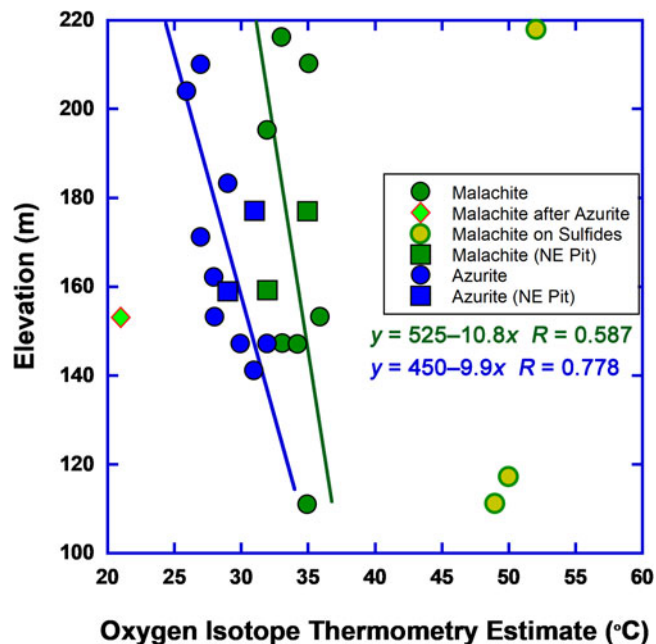


**Fig. 5.** Oxygen isotope thermometry estimates for copper carbonate samples shown vs. depth in the deposit as metres elevation above reference. Trend lines exclude pseudomorphs and carbonate on sulfide.

Copper carbonate samples from the Girilambone deposits have carbon isotope values similar to many deposits where chemolithophile bacteria are known to play an important role in the breakdown of sulfide minerals within the oxidation zone. In fact, the Girilambone values for both azurite and malachite show a similar ‘main trend’ to the malachite reported in Melchiorre and Enders (2003) with slightly lighter values at higher elevations within the oxidation zone (Fig. 6). This is consistent with mixing between an isotopically light bacterial carbon source and atmospheric carbon.

The exceptions to this general behaviour are the malachite observed as pseudomorphs after azurite, and malachite growing on the sulfide samples. The  $\delta^{13}\text{C}$  value of the malachite pseudomorph after azurite is the heaviest of all at -6.6‰, while the malachite growths on massive sulfide were the lightest of all with an average of -14.9‰. These variations are several permil (‰) different from the ‘main trend’ of values (Fig. 6).

These values for malachite that deviate from the main trend still convey formation conditions consistent with field observations of the conditions of formation. The malachite pseudomorph sample has a  $\delta^{13}\text{C}$  value which is consistent with pre-industrial atmospheric values of -6.5 to -7.0‰ (Saurer *et al.*, 1997; Grocke, 2002; McCarroll and Loader, 2004; Leuenberger, 2007). It is known from textural relationships that the malachite pseudomorph sample formed late in the paragenetic sequence when most primary sulfides above the water table would have already been digested by a combination of metal-metabolising chemolithophile bacteria and inorganic chemical reactions. Carbon isotope values of pore gasses at this time would be more likely to reflect atmospheric or soil carbonate values.

For the malachite growths on sulfide minerals, the  $\delta^{13}\text{C}$  values are much lighter with an average of -14.9‰. These values are consistent with a probable carbon source of metal-metabolising chemolithophile bacteria broadly characterised as ‘Thiobacillus

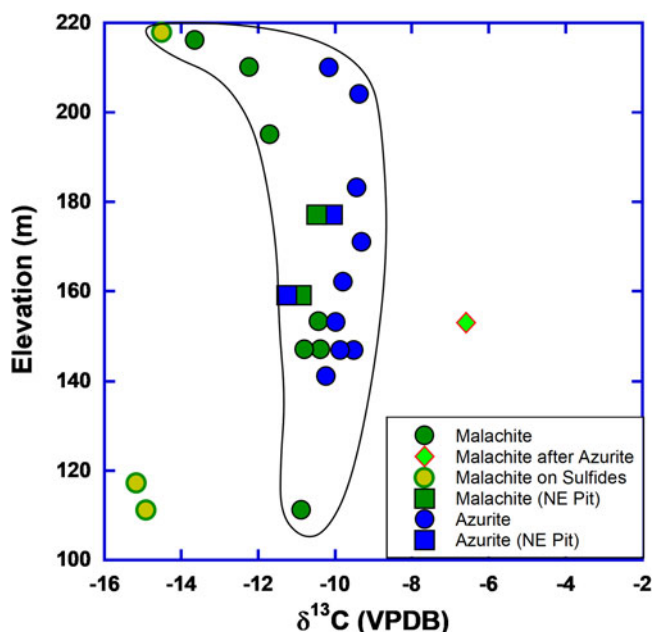


**Fig. 6.** Carbon isotope values for copper carbonate samples shown vs. depth in the deposit as metres elevation above reference. The bag-plot encloses the trend of lower carbon isotope values near the surface. This trend encloses one of the sulfide-hosted samples that was obtained from old mine workings on the surface, while the two sulfide-hosted samples outside of this trend were from a deep portion of the deposit that presumably were exposed and oxidised much more recently.

ferrooxidans' as documented at Morenci, Arizona, USA (Melchiorre and Enders, 2003) and Great Australia, Queensland, Australia (Melchiorre and Williams, 2001). The observed rapid rate of decomposition of these sulfides and their exothermic behaviour are also consistent with bacterial decomposition of sulfides.

### Chlorine isotope implications

The formation of atacamite-group minerals (referred to here as 'atacamite') from groundwater flowing from pit seeps along the northern side of the Murrawombie pit presents yet another opportunity to examine conditions of secondary mineral formation in the deposit. Significantly, older atacamite was only documented from a single sample at Girilambone, and that sample was from a stockpile and thus has no context for its original position in the oxidation zone (Chapman *et al.*, 2005). This nearly complete absence of atacamite and other chloride minerals (including pseudomorphs that might indicate their past presence) at Girilambone is interpreted to reflect the low relative chloride activities during formation of the oxide zone (Williams, 1990). The formation of atacamite in the active mining environment suggests a change in groundwater or pore fluid chemistry since the development of the oxidation zone.

The  $\delta^{37}\text{Cl}$  (SMOC) value of modern-forming atacamite at Girilambone (+0.25‰) is an exact match for the value reported for pyromorphite from Broken Hill, Australia and a close match for many evaporite and some oxidation zone minerals (Eggenkamp and Schuiling, 1995). Significantly, Eggenkamp and Schuiling (1995) concluded that high values of  $\delta^{37}\text{Cl}$  up to +6‰ for atacamite, boleite and connellite were the result of formation early in the development of the oxidation zone when sulfide decomposition produced low pH. These low pH conditions

liberated chlorine gas with attendant fractionation to elevate pore water  $\delta^{37}\text{Cl}$  values. The near-zero chlorine isotope values were interpreted by Eggenkamp and Schuiling (1995) to result from a seawater chloride source, and/or formation late in formation of the oxidation zone when pH values have risen as sulfide oxidation nears completion. The  $\delta^{37}\text{Cl}$  value for Girilambone atacamite is also consistent with values reported for the groundwater of the Great Artesian Basin of Australia (Zhang *et al.*, 2007), which concluded that chloride was sourced from marine aerosols and not the dissolution of sedimentary salt. This would potentially explain the non-seawater major-ion ratios of seep water (Table 2), though diagenetic processes could also explain the water chemistry differences. The Girilambone atacamite value is also consistent with atacamite from Chile at depths of ~50 m within the oxidation zone where deep sedimentary basin brine and freshwater mixing is suspected (Reich *et al.*, 2008; 2019).

### Girilambone oxide deposit genesis

Though there is evidence that some of the development of the oxidation zone at Girilambone occurred in stages coincident with minor water-table fluctuations and erosion, the dominant stage of oxidation appears to have been a single protracted event under relatively stable conditions. During this event, secondary chalcocite formed a main enrichment blanket at and near the present water-table elevation. At these same levels and above, cuprite and native copper dominate in a transition zone (Fig. 4).

Above the transition zone, basic copper carbonates are typically the main copper minerals. Isotopic evidence from malachite growing on copper sulfide samples from the eastern shear lode suggest elevated temperatures of formation (~50°C, from oxygen isotope values), probably due to exothermic decomposition of sulfides by chemolithotrophic bacteria (recorded as  $\delta^{13}\text{C} \approx -14.9\text{‰}$ ). Temperatures in this range are consistent with rapid oxidation, such as that observed when the chalcocite blanket was exposed at the Gunpowder mine in Queensland, Australia. During fieldwork at the Gunpowder mine, the author, Peter Williams, Jim Sharpe and Vera Munro-Smith could barely walk across the ~50°C ground which rapidly heated boot soles to unbearable levels. At Girilambone, these malachite-on-sulfide samples have grown in a post-mining environment and are interpreted as representing a potential end-member environment for the oxidation zone forming directly at the interface with decomposing masses of sulfide minerals.

The main stage of malachite formation records much lower temperatures of 32 to 36°C (Table 1). These values are still well above ambient air temperatures, but below that recorded by malachite on sulfides. This suggests malachite formation following peak sulfide decomposition and attendant heat dissipation, or formation at a greater distance from the exothermic sulfide decomposition. These same malachite samples show a trend of increasingly lighter  $\delta^{13}\text{C}$  values towards the pre-mining surface (Fig. 6). This may result from a light surficial carbon source, or preserve the upwards diffusive loss of  $\text{CO}_2$  from a deep source as an isotope gradient. It is suggested that the most plausible scenario is the exothermic decomposition of deep sulfides adjoining the water table to produce thermal and carbon isotope gradients.

Similar trends are observed for azurite samples. Azurite temperatures are slightly lower than for malachite (27 to 32°C) and may indicate formation later than most malachite, when thermal decomposition of sulfides was waning. This is consistent with

paragenetic relations noted in hand samples of Girilambone copper carbonate ores. Weak trends of increasing temperature with increasing depth for all main-stage copper carbonates indicate a thermal source at the water table, consistent with formation of the enrichment blanket and dissolution of primary sulfides. Azurite also has slightly heavier carbon isotope values, but a similar profile with depth in comparison to malachite. Both azurite and malachite samples from the main stage have carbon isotope values similar to other localities where microbial carbon is believed to be a significant carbon source (e.g. Melchiorre and Williams, 2001; Melchiorre and Enders, 2003). The malachite pseudomorph after azurite, arguably the last mineral to form in the main paragenetic sequence examined in this study, has the lowest temperature of formation and the heaviest carbon isotope value. These values are similar to modern ambient air temperatures and pre-industrial atmospheric carbon values (Saurer *et al.*, 1997; Grocke, 2002; McCarroll and Loader, 2004; Leuenberger, 2007).

It is suggested that the sequence of copper carbonate mineral formation followed a general trend. Malachite formation was first, as temperatures within the deposit were still quite warm from decomposition of primary sulfides. As malachite and other minerals formed, they progressively sealed fracture networks which restricted the discharge of CO<sub>2</sub> and other gases produced by decomposition of sulfides by chemolithotrophic bacteria, similar to that recorded by Melchiorre and Enders (2003). Of special importance was the formation of white and red clays (notes in Table 1). Veins and zones of azurite generally occur following malachite and in close association with these clays, similar to observations of this association made by the author at copper deposits across the southwestern USA and some locations in Australia (full discussion on page 179 in Melchiorre *et al.*, 2017 and references therein). It has been known for many years that malachite will often form before azurite in copper deposits where both minerals occur (e.g. Schwartz, 1934). This trend of malachite formation before azurite probably records the changing partial pressures of CO<sub>2</sub>, where rising CO<sub>2</sub> levels pass through the stability field of malachite and into the stability field of azurite (see figure 14 in Melchiorre *et al.*, 2017).

The typical partial pressure of CO<sub>2</sub> in the atmosphere is  $\sim 10^{-3.5}$  atmospheres, which dictates that malachite will be the more stable carbonate (e.g. Williams, 1990). An increase in CO<sub>2</sub> pressure to  $10^{-1.36}$  atmospheres or higher would result in the formation of azurite (e.g. Williams, 1990; Kiseleva *et al.*, 1992). It is suggested that the generation of impermeable clay during weathering of the oxidation zone elevates p[CO<sub>2</sub>] levels by creating a comparatively closed system that can reach the high levels above atmospheric levels required for azurite formation. In some cases, the clay may be associated with a fault gouge (Melchiorre and Enders, 2003), while in others it may be associated with weathering of primary lithology (Melchiorre *et al.*, 2017). Regardless of origin, clay is clearly associated with azurite in the Girilambone deposits. It is suggested that these clays in the oxidation zone at Girilambone reduced the ability of CO<sub>2</sub> generated by chemolithotrophic bacteria to escape upwards to the atmosphere. Initial development of the oxidation zone occurred in a system that was essentially open to the atmosphere and favoured formation of malachite. As secondary minerals, and especially clays, reduced permeability the partial pressures of CO<sub>2</sub> rose into the stability field of azurite. However, this was not a closed system, and the leakage of CO<sub>2</sub> produced isotopic fractionation by diffusion as lighter carbon was selectively lost towards the surface. The downward migration

of fluids and the upward loss of CO<sub>2</sub> became concentrated within specific sectors within the oxidation zone such as large fracture zones and permeable units. The result was formation of azurite higher in the oxidation zone than would be expected, within these structurally dictated pockets of elevated CO<sub>2</sub>. Similar 'blow-out' zones related to diagenetic compaction were noted in other deposits (Melchiorre *et al.*, 2017). Fluctuations in CO<sub>2</sub> partial pressure probably occur when new pathways opened and old ones closed. However, the interbanding of azurite and malachite that would be produced by seasonal rains or frequent fluctuations (e.g. Melchiorre and Enders, 2003) are not commonly observed at Girilambone. It is also possible that erosion plays some role in the azurite formation at such apparently shallow depths in the oxidation zone. However the levels of erosion relative to the timing of deposit oxidation remain unquantified.

As sulfides were consumed by exothermic oxidation and bacterial digestion, generation of CO<sub>2</sub> waned and temperatures decreased. It was on this 'retrograde' side of maximum deposit oxidation that pseudomorphs of malachite after azurite began to form at essentially atmospheric temperatures and with pre-industrial atmospheric carbon isotope values. Eventually, CO<sub>2</sub> production decreased to a point that the pre-existing chemistry of the local groundwater once again dominated the system. It is in this latest period that atacamite precipitation occurs as chloride-rich groundwater interacts with copper-rich oxidation fluids. It is possible that the documentation of a single sample of atacamite at Girilambone (Chapman *et al.*, 2005) records an early period of weak weathering before CO<sub>2</sub> began to dominate the system. However, that lone sample was from a stockpile and thus has no context for its original position in the oxidation zone or attendant paragenetic relationships.

It bears mentioning that the single dominant phase of oxidation suggested by the evidence is of unknown duration. It may have persisted for long enough to give the appearance of separate events, as evidenced by overprints of early malachite with later azurite overgrowths, which in turn was altered in places back to malachite pseudomorphs. This protracted period of oxidation and attendant mineralogical zonation could be interpreted as either temporal or spatial zonation. However, the documentation of deep intense weathering and the isotopic gradients measured with depth in the deposit suggest this was a single event that records a protracted period of oxidation-zone weathering reactions, and not discrete unrelated events.

Future workers should consider examining the relationship between the regional weathering history and the events captured during oxidation of the deposit. Without data on ages for the different levels of the weathering profiles at Girilambone it is difficult to reconcile the genesis stages indicated by this study and those of the regional weathering history. However, regional weathering history suggests that most of the weathering preserved at Girilambone would predate the Mid Miocene (17 Ma). The predominantly arid to semi-arid conditions following this period would generate more limited chemical weathering, as indicated by the relatively unweathered Miocene leucites, which sit on a deeply weathered profile at Wilga Tank 65 km west of Girilambone (McQueen *et al.*, 2007).

## Conclusions

The Girilambone deposit is a textbook example of a classic oxidation zone profile. Unlike the oxidation profiles of porphyry copper deposits of western North America which have been

overprinted by water-table fluctuations produced by active tectonics, the Girilambone deposit appears to have little modification to the original oxidation profile.

Oxidation of primary sulfides at Girilambone was an exothermic process facilitated by chemolithotrophic bacteria. The bacteria generated CO<sub>2</sub> which migrated upwards to react with copper rich meteoric fluids of the vadose zone to precipitate malachite. Over time, secondary minerals like clays, iron oxides and basic copper carbonates reduced permeability of the oxidation zone. Unlike porphyry copper deposits of western North America, this deposit did not experience significant tectonic activity during oxidation to re-establish permeability. Thus the reduced permeability slowed the release of CO<sub>2</sub> from the system and produced significantly elevated partial pressure of CO<sub>2</sub> that was sufficient for azurite formation to dominate the system. The bacteria populations at Girilambone also appear to have been stable over time and not seasonal, as the deposit has no interbanded azurite and malachite typical of episodic bacterial populations triggered by seasonal precipitation (e.g. Melchiorre and Enders, 2003). The absence of significant Cu-carbonate banding at Girilambone may therefore serve as a palaeoclimate indicator. Deeper in the Girilambone oxidation zone, native copper and cuprite dominate, whereas chalcocite formed an enrichment blanket just above and at the modern water table. Eventually, as CO<sub>2</sub> production from bacterial digestion of sulfides waned, pseudomorphs of malachite after azurite were generated as a retrograde reaction. In the modern Girilambone operations, local chloride-rich groundwater emerges as pit weeps which precipitate atacamite, while exposed remnants of sulfide masses form a rind of porous malachite. Local channelisation of fluids and perched water-table lenses generated exceptions to this oxidation zone sequence and created mineralogical overprints.

The Girilambone deposit thus serves as an end-member model for the development of an oxidation zone in an environment virtually free of the effects of active tectonics and significant fluctuation in the local water table. It is suggested that the oxidation zone of other deposits may be interpreted for history of recently active tectonics, palaeoclimate, and water table stability by comparison to the Girilambone deposit.

**Acknowledgments.** This paper would not have been possible without the help of three talented mining professionals who realize the benefit of research to their industry. First, Phil Shields provided generous time and expertise towards understanding the geology of the deposit and the collection of samples. Tony Thomas and Mark Welch provided administrative support for this project and guest lodging for the author. Specific thanks go to Peter Williams for his two decades of friendship and intellectual support of research projects on copper deposits of Australia. Instrumentation used in this study was provided by generous grants from the National Science Foundation, the W.M. Keck Foundation, and an internal VETI Grant by CSUSB. Travel support was provided by National Science Foundation International Travel Program. Greg Holk at CSU Long Beach provided access to carbonate stable isotope instrumentation. Jim Sickman and Delores Lucero at University of California Riverside provided chlorine analysis instrumentation and expertise. Anonymous reviewer #3 provided a wealth of useful information regarding the regional weathering history.

## References

- Aeris Resources Limited (Brisbane, Queensland, Australia) (2021) Accessed from <https://www.aerisresources.com.au/operations/tritton-copper-operations/#murrawombie-underground> on 08/04/2021.
- Bowen R. (1966) Oxygen isotopes as climatic indicators. *Earth-Science Reviews*, **2**, 199–224.
- Carne J.E. (1908) *The Copper Mining Industry*. New South Wales Department of Mines, 6, pp. 570.
- Chapman J.R., Sharpe J.L. and Williams P.A. (2005) The copper deposits at Girilambone, New South Wales. *Australian Journal of Mineralogy*, **11**, 91–99.
- Coleman M.L., Shepherd T.J., Durham J.J., Rouse J.E. and Moore G.R. (1982) Reduction of water with zinc for hydrogen isotope analysis. *Analytical Chemistry*, **54**, 993–995.
- Coplen T.B. (1995) Discontinuance of SMOW and PDB. *Nature*, **375**, 285.
- Crane M.J., Sharpe J.L. and Williams P.A. (2001) Formation of chrysocolla and secondary copper phosphates in the highly weathered supergene zones of some Australian deposits. *Records of the Australian Museum*, **53**, 49–56.
- Eggenkamp H.G.M. and Schuiling R.D. (1995) δ<sup>37</sup>Cl variations in selected minerals: a possible tool for exploration. *Journal of Geochemical Exploration*, **55**, 249–255.
- Eggenkamp H.G.M., Middelburg J.J. and Kreulen R. (1994) Preferential diffusion of <sup>35</sup>Cl relative to <sup>37</sup>Cl in sediments of Kau Bay, Halmahera, Indonesia. *Chemical Geology*, **116**, 317–325.
- Epstein S. and Mayeda T. (1953) Variation of O18 content of waters from natural sources. *Geochimica et Cosmochimica Acta*, **4**, 213–224.
- Fogarty J.M. (1996) Exploration for leachable copper deposits Girilambone district. Pp 179–193 in: *The Cobar Mineral Field – A 1996 Perspective* (W.G. Cook, A.J.H. Ford, J.J. McDermott, P.N. Standish, C.L. Stegman and T.M. Stegman, editors). The Australasian Institute of Mining and Metallurgy, Melbourne, Australia.
- Fogarty J.M. (1998) Girilambone district copper deposits. Pp 593–600 in: *Geology of Australian and Papua New Guinean Mineral Deposits* (D.A. Birkman and D.H. Mackenzie, editors). The Australasian Institute of Mining and Metallurgy, Melbourne, Australia.
- Grocke D.R. (2002) The carbon isotope composition of ancient CO<sub>2</sub> based on higher-plant organic matter. *Philosophical Transactions of the Royal Society of London*, **A360**, 633–658.
- Khider K. and McPhail D.C. (2005) Hydrogeology and hydrogeochemistry in the Hermidale area, NSW. Pp. 165–169 in: *Ten years of CRC LEME*. Cooperative Research Centre for Landscape Environments and Mineral Exploration, Australia.
- Kiseleva I.A., Ogorodova L.P., Melchakova L.V., Bisengaliyeva M.R. and Becturganov N.S. (1992) Thermodynamic properties of copper carbonates—malachite Cu<sub>2</sub>(OH)<sub>2</sub>CO<sub>3</sub> and azurite Cu<sub>3</sub>(OH)<sub>2</sub>(CO<sub>3</sub>)<sub>2</sub>. *Physics of Chemistry and Mineralogy*, **19**, 322–333.
- Leuenberger M. (2007) To what extent can ice core data contribute to the understanding of plant ecological developments in the past? *Terrestrial Ecology*, **1**, 211–233.
- McCarroll D. and Loader N.J. (2004) Stable isotopes in tree rings. *Quaternary Science Reviews*, **23**, 771–801.
- McQueen K. (2018) Copper under the stars: The history of discovery and mining at Girilambone, northwest New South Wales. *Journal of Australasian Mining History*, **16**, 127–147.
- McQueen K.G., Gonzalez O.R., Roach I.C., Pillans B.J., Dunlap W.J. and Smith M.L. (2007) Landscape and regolith features related to Miocene leucite lava flows, El Capitan northeast of Cobar, NSW. Australia. *Australian Journal of Earth Sciences*, **54**, 1–17.
- McQueen K.G., Chan R.A., Khider K. Greene R.S.B. and Scott K.M. (2008) *Regolith architecture and geochemistry of the Girilambone region, north-western New South Wales – A synthesis Report*. CRC LEME Open File Report 215, 57 pp and CD database [has a summary table on all weathering related dates].
- Melchiorre E.B. and Enders M.S. (2003) Stable isotope geochemistry of copper carbonates at the Northwest Extension Deposit, Morenci District, Arizona: implications for conditions of supergene oxidation and related mineralization. *Economic Geology*, **98**, 607–621.
- Melchiorre E.B. and Williams P.A. (2001) Stable isotope characterization of the thermal profile and subsurface biological activity during oxidation of the Great Australia deposit, Cloncurry, Queensland, Australia. *Economic Geology*, **96**, 1685–1693.
- Melchiorre E.B., Criss R.E. and Rose T.P. (1999) Oxygen and carbon isotope study of natural and synthetic malachite. *Economic Geology*, **94**, 245–259.

- Melchiorre E.B., Criss R.E. and Rose T.P. (2000) Oxygen and Carbon Isotope Study of Natural and Synthetic Azurite. *Economic Geology*, **95**, 621–628.
- Melchiorre E.B., McLaughlin D., Bottrill R. and Hight J. (2017) Primary diagenetic copper carbonate at the Malbunka copper deposit, Amadeus Basin, Northern Territory, Australia. *Ore Geology Reviews*, **82**, 170–180.
- Reich M., Palacios C., Parada M.A., Fehn U., Cameron E.M., Leybourne M I. and Zúñiga A. (2008) Atacamite formation by deep saline waters in copper deposits from the Atacama Desert, Chile: evidence from fluid inclusions, groundwater geochemistry, TEM, and  $^{36}\text{Cl}$  data. *Mineralium Deposita*, **43**, 663.
- Reich M., Barnes J.D., Breecker D.O., Barra F., Milojevic C. and Drew D.L. (2019) Chlorine isotope fractionation recorded in atacamite during supergene copper oxidation. *Chemical Geology*, **525**, 168–176.
- Saurer M., Borella S., Schweingruber F. and Siegwolf R. (1997) Stable carbon isotopes in tree rings of beech: climatic versus site-related influences. *Trees*, **11**, 291–297.
- Schwartz G. M. (1934) Paragenesis of the oxidized ores of copper. *Economic Geology*, **29**, 55–75.
- Shields P. (1996) Geology of the Girilambone copper deposit. Pp. 293–304 in: *The Cobar Mineral Field – A 1996 Perspective* (W.G. Cook, A.J.H. Ford, J.J. McDermott, P.N. Standish, C.L. Stegman and T.M. Stegman, editors). The Australasian Institute of Mining and Metallurgy, Melbourne, Australia.
- Smith M.L., Pillans B.J. and McQueen K.G. (2009) Palaeomagnetic evidence for periods of intense oxidative weathering, McKinnons Mine, Cobar, NSW. *Australian Journal of Earth Science*, **56**, 201–212.
- Straits Resources (2003) Annual Shareholders Report: Girilambone Copper Project. Archived from <http://www.straits.com.au/operations/girilambone.htm> on 11/09/2004, link no longer accessible.
- Williams P.A. (1990) *Oxide Zone Geochemistry*. Ellis Horwood, UK, 286 pp.
- Zhang M., Frapé S.K., Love A.J., Herczeg A.L., Lehmann B.E., Beyerle U. and Purtschert R. (2007) Chlorine stable isotope studies of old groundwater, southwestern Great Artesian Basin, Australia. *Applied Geochemistry*, **22**, 557–574.